Developmental Biology 386 (2014) 12–24

Contents lists available at ScienceDirect

Developmental Biology

journal homepage: www.elsevier.com/locate/developmentalbiology

The *Arabidopsis thaliana GRF-INTERACTING FACTOR* gene family plays an essential role in control of male and female reproductive development

Byung Ha Lee [a,1], April N. Wynn [b,2], Robert G. Franks [b], Yong-sic Hwang [c], Jun Lim [c], Jeong Hoe Kim [a,*]

[a] Department of Biology, Kyungpook National University, Daegu 702-701, Republic of Korea
[b] Department of Plant and Microbial Biology, North Carolina State University, Raleigh, NC 27695, USA
[c] Department of Bioscience and Biotechnology, Konkuk University, Seoul 143-701, Republic of Korea

ARTICLE INFO

Article history:
Received 29 October 2013
Received in revised form
27 November 2013
Accepted 9 December 2013
Available online 16 December 2013

Keywords:
Arabidopsis thaliana
GRF-INTERACTING FACTOR
Carpel
Anther
Cell specification

ABSTRACT

Reproductive success of angiosperms relies on the precise development of the gynoecium and the anther, because their primary function is to bear and to nurture the embryo sac/female gametophyte and pollen, in which the egg and sperm cells, respectively, are generated. It has been known that the GRF-INTERACTING FACTOR (GIF) transcription co-activator family of *Arabidopsis thaliana* (*Arabidopsis*) consists of three members and acts as a positive regulator of cell proliferation. Here, we demonstrate that GIF proteins also play an essential role in development of reproductive organs and generation of the gamete cells. The *gif*1 *gif*2 *gif*3 triple mutant, but not the single or double mutants, failed to establish normal carpel margin meristem (CMM) and its derivative tissues, such as the ovule and the septum, resulting in a split gynoecium and no observable embryo sac. The *gif* triple mutant also displayed severe structural and functional defects in the anther, producing neither microsporangium nor pollen grains. Therefore, we propose that the GIF family of *Arabidopsis* is a novel and essential component required for the cell specification maintenance during reproductive organ development and, ultimately, for the reproductive competence.

Introduction

Plant seeds are carriers of an embryo from which a plant starts a new life cycle. In angiosperms, flowers are pivotal reproductive organs for fertilization and setting seeds, allowing the generation-to-generation continuity. Reproductive success of angiosperms is contingent on the normal development of the gynoecium and the anther, which bear and house the female and male gametophytes, respectively.

The gynoecium of *Arabidopsis thaliana* (*Arabidopsis*) is composed of four distinctive regions at maturity: stigma, style, ovary, and gynophore (Ferrándiz et al., 1999, 2010). The ovary has discernible exterior portions along its longitudinal axis, i.e., two lateral carpels and two medial repla. Two carpels are congenitally fused together from their earliest emergence and are separated only by an intervening tissue, the septum, forming a bilocular chamber. The replum is the external part of the septum and marks exterior boundaries between carpel valves. Apically the ovary meets the style that is topped with the stigma, and while basally it meets the gynophores. Internally, the gynoecium consists of placenta, ovule, septum, and transmitting tract (Ferrándiz et al., 1999, 2010). Importantly, all of those internal tissues, as well as medial portions of the style and the stigma, originate from the carpel margin meristems (CMMs), meristematic structures that arise from the medial portions of the gynoecium primordium (Bowman et al., 1999; Azhakanandam et al., 2008).

Ovule development is completed through four main events: (1) primordium initiation and elongation from the placenta; (2) regionalization of primordium into three zones, i.e., funiculus, chalaza, and nucellus; (3) initiation and growth of integuments from the chalazal region; and (4) development of the embryo sac from the megaspore mother cell (MMC) (Bouman, 1984; Reiser and Fischer, 1993). The MMC, which is initially specified as the archesporial cell in the nucellus, performs the sporogenesis and gametogenesis consecutively to generate the embryo sac, thus giving rise to an egg cell and other gametophytic cells (Webb and Gunning, 1990; Yadegari and Drews, 2004).

Pollen grains are male gametophytes developing within microsporangia that reside within four lobes of the anther (Sanders et al., 1999). Each microsporangium consists of three outer concentric parietal layers – endothecium, middle layer, and tapetum – and

* Corresponding author. Fax: +82 53 953 3066.
E-mail addresses: kimjeon4@knu.ac.kr, kimjeon4@mail.knu.ac.kr (J.H. Kim).
[1] Present address: Department of Plant Biology, University of Minnesota, St. Paul, MN 55108, USA
[2] Present address: Department of Biology, St. Mary's College of Maryland, St. Mary's City, MD 20686, USA

0012-1606/$ - see front matter © 2013 Elsevier Inc. All rights reserved.
http://dx.doi.org/10.1016/j.ydbio.2013.12.009

harbors pollen mother cells (PMCs) in the center. All those parietal layers and PMCs are mitotic progeny of the archesporial cells that are earlier specified in the L2 layer of the stamen primordium (Sanders et al., 1999). PMCs, like MMC, perform the sporogenesis and gametogenesis consecutively and generate pollen grains containing two sperm cells and a vegetative cell. Therefore, establishment of the female and male gametophytes, together with that of the gynoecium and the anther in which they develop, is of pivotal importance for reproductive competence of angiosperms, including *Arabidopsis*.

We have previously uncovered a small family of transcriptional co-activators, GRF-INTERACTING FACTOR (GIF), in *Arabidopsis*. The GIF protein family comprises three members that form a functional complex with the GROWTH-REGULATING FACTOR (GRF) transcriptional factors (Kim et al., 2003; Kim and Kende, 2004; Horiguchi et al., 2005; Lee et al., 2009). GIF1 (also called *ANGUSTIFOLIA*3, *AN*3), GIF2 and GIF3 are all required for lateral organ growth, and act as positive regulators of cell proliferation in a functionally redundant manner. In short, the loss-of-function mutations in the *GIF*1/*AN*3 gene, *gif*1 and *an*3, resulted in small, narrow leaves and petals with a small number of cells. Although the *gif*2 and *gif*3 loss-of-function mutants displayed no obvious developmental phenotypes, double and triple combinations between *gif*1, *gif*2, and *gif*3 displayed a remarkably synergistic decrease in the sizes and cell numbers of lateral organs.

When performing genetic analyses in regard to lateral organ growth, we noticed that the *gif*1 *gif*2 *gif*3 triple mutant, but no single and double mutants, developed split gynoecia. Here, we demonstrate that the *gif* triple mutant displays severe structural and functional defects in the CMM and its derivatives (collectively, CMM tissues) as well as in the anther. Histological analyses revealed that, in the *gif* triple mutant, meristematic cells of the CMM tissues and the functional megaspore fail to develop properly, resulting in split gynoecia and a disruption of embryo sac development. Furthermore, the archesporial lineage cells in the mutant anther failed to produce the microsporangium, PMCs, and pollen. Therefore, we propose that the *GIF* family of *Arabidopsis* is a novel and essential component required for the development of the male and female reproductive structures and gametes.

Materials and methods

Plant materials

Wild-type *A. thaliana* (L.) Heynh plants were used, and all of the *gif* mutants are in the same accession (Lee et al., 2009). Growth conditions were described in Lee et al. (2009).

Scanning electron microscopy (SEM)

Flower clusters were harvested into a FAA solution (5 ml of ethanol, 0.5 ml of acetic acid, 1 ml of 37% formaldehyde, 3.5 ml of distilled water). The samples were incubated under vacuum (550 mmHg) and were transferred to a fresh FAA solution at 4 °C. Next day, the fixative was replaced with an OsO_4 solution (1 g of OsO_4 in 100 ml of 25 mM sodium phosphate buffer, pH 7.2; Heraeus, South Africa). The samples were incubated at 4 °C overnight, then rinsed with sodium phosphate buffer three times, dehydrated through an ethanol series at room temperature and stored in 100% ethanol before use. After the critical point dry (HCP-2 critical point dryer, Hitachi, Japan), the samples were mounted on stubs, coated with gold particles, and subjected to SEM (S-4300 & EDX-350, Hitachi, Japan).

Histological analysis

Flower clusters were fixed as mentioned above, washed with 1 × PBS (0.13 M NaCl, 7 mM Na_2HPO_4, 3 mM NaH_2PO_4, pH7.0) for 30 min twice, and dehydrated in a graded ethanol series, after which ethanol was replaced with a mixture of an equal volume of ethanol and Histoclear (National diagnostics, USA), then with Histoclear alone three times, and finally with a mixture of a third of Histoclear and two thirds of solid paraplast chips (Merck, Germany). The samples were stored at room temperature overnight and incubated further at 60 °C for 2 h. The last step was repeated three times with freshly melted paraplast. The samples were transferred to a plastic mold (Simport, Canada). Tissue blocks were sectioned 8 μm in thickness by a microtome (Leica RM2125RT, Germany). Tissue sections were stained with 0.1% toluidine blue O, except the *GUS* transgenic flowers (Sigma-Aldrich, USA).

Differential interference contrast microscopy (DIC)

Flower clusters were fixed with ethanol: acetic acid (6:1) and were washed with 100% ethanol three times and then with 70% ethanol once. The flower samples were cleared in a chloral hydrate solution (8 g of chloral hydrate, 1 ml of glycerol, and 2 ml of distilled water), and their images were obtained using a light microscope (Eclipse NI-U, Nikon, Japan).

Construction of GIFpro::GIF::GUS transgenic plants

Genomic DNA of the wild-type plant was amplified by PCR using primer pairs (see Supplementary Table 1). Amplified DNAs of *GIF*1, *GIF*2, and *GIF*3 included the promoter, introns, and exons except the stop codon, and were approximately 2.9, 1.8, and 1.7 kbp in length, respectively. It should be noticed that the promoters of *GIF*2 and *GIF*3, including 5′ untranslated region, are extremely short (396 and 291 base pairs, respectively), because they are closely adjoined, in a head-to-head manner, to neighboring genes (At1g01150 and At4g00840, respectively; Supplementary Fig. 1). After digestion with *Sal*I and *Xba*I, PCR products were put in frame to the β-*glucuronidase* (*GUS*) gene of the *pBI*101.1 vector according to In-Fusion™ Advantage PCR Cloning Kit (Clontech, USA), resulting in the *GIF-GUS* translational fusion constructs. Those constructs were introduced into *Arabidopsis* plants by the *Agrobacterium tumefaciens*-mediated transformation (Clough and Bent, 1998). Dozens of independent T_1 plants for each construct were selected on MS agar plates (0.5 × Murashige-Skoogs salts, 1% sucrose, 0.8% phytoagar, 50 μg/ml kanamycin; all from Duchefa Biochemie, the Netherlands, except sucrose, which was from Amresco, USA). Single-insertion lines were subjected to the GUS staining procedure. All of the lines for each construct showed an identical staining pattern and, therefore, a typical pattern was presented.

Procedures for in situ hybridization and GUS staining

Gene-specific DNA region was amplified by PCR using primer pairs (see Supplementary Table 1) and ligated into the *pGEM-T* (for GIF1) or *pGEM-Teasy* (GIF2 and GIF3) vector (Promega, USA). Production of anti-sense probes was achieved by in vitro transcription from SP6 (GIF1 and GIF3) or T7 (GIF2) promoter. The in situ hybridizations were carried out as reported previously (Wynn et al., 2011). The GUS staining procedure was performed according to Rodrigues-Pousada et al. (1993) with a slight modification.

Results

Exterior defects in the gynoecium and the anther of the gif triple mutant

As mentioned above, the *gif*1 *gif*2 *gif*3 triple loss-of-function mutant displayed aberrant gynoecia, which prompted us to investigate the role of the *GIF* family in floral organ development. The *gif* triple mutant had fewer petals and stamens than the wild-type plant, whereas the *gif* double mutants, i.e., *gif*1 *gif*2, *gif*2 *gif*3, and *gif*1 *gif*3, showed no difference (Table 1). Although the triple mutant had two carpels as the wild-type plant did, its carpels failed to fuse, resulting in split gynoecia (Table 1; Fig. 1). In addition, unusual organs, such as stamenoid petals and petaloid stamens, arose in the second and third whorls of flowers, but with the frequency less than 1% of flowers examined (Fig. 1X and Y).

We compared gynoecial development of *gif*1 *gif*2 *gif*3 with the wild type. Wild-type flower buds were tightly wrapped with partially overlapping sepals until anthesis, whereas those of the *gif* triple mutant were not, because sepal growth was retarded, exposing split gynoecium (Fig. 1A and H). In order to understand when and how the gynoecium defect arises, we examined the morphological development of wild-type and mutant gynoecia. The wild-type gynoecial primordium starts to form in the center of the floral meristem, immediately after peripheral initiation of stamens at flower stage 5 (Fig. 1B; Smyth et al., 1990). As the gynocium primordium grows further to stage 8, it takes a cylindrical structure, being hollowed in a slotted form (Fig. 1C and D). The hollow cylinder then closes at the apex by being topped with papillary cells, first on the medial surface and afterwards over the entire surface of the gynoecium, culminating in completion of the stigma (Fig. 1E, F, and F′). During that period, the gynoecial tissue just beneath the stigma differentiates into the style, leading to the mature gynoecium (Fig. 1F and F′). At stage 12, two carpel valves of the ovary were clearly distinguished by the intervening tissue, the replum (Fig. 1F and F′). During the earliest

Table 1
Numbers of floral organs and ovules [a].

	Sepal	Petal	Stamen	Carpel	Split carpel (%)	Ovules
WT	4.00 ± 0.00	4.00 ± 0.00	5.99 ± 0.01	2.00 ± 0.00	0	51.4 ± 0.21
*gif*1 *gif*2	4.00 ± 0.00	3.99 ± 0.00	5.98 ± 0.01	2.00 ± 0.00	0	26.6 ± 0.67
*gif*2 *gif*3	4.00 ± 0.00	4.00 ± 0.00	5.95 ± 0.02	2.00 ± 0.00	0	52.2 ± 0.48
*gif*1 *gif*3	3.99 ± 0.00	4.00 ± 0.00	5.98 ± 0.01	2.00 ± 0.00	0	33.2 ± 0.52
*gif*1 *gif*2 *gif*3	3.99 ± 0.03	2.15 ± 0.03	4.41 ± 0.04	2.00 ± 0.04	100	13.2 ± 0.43

[a] The first to 15th flowers were analyzed. Values are means ± s.e.m. $n = 210$ for WT; 375 for *gif*1 *gif*2; 210 for *gif*2 *gif*3 and *gif*1 *gif*3; 465 for *gif*1 *gif*2 *gif*3; 10 siliques for ovules.

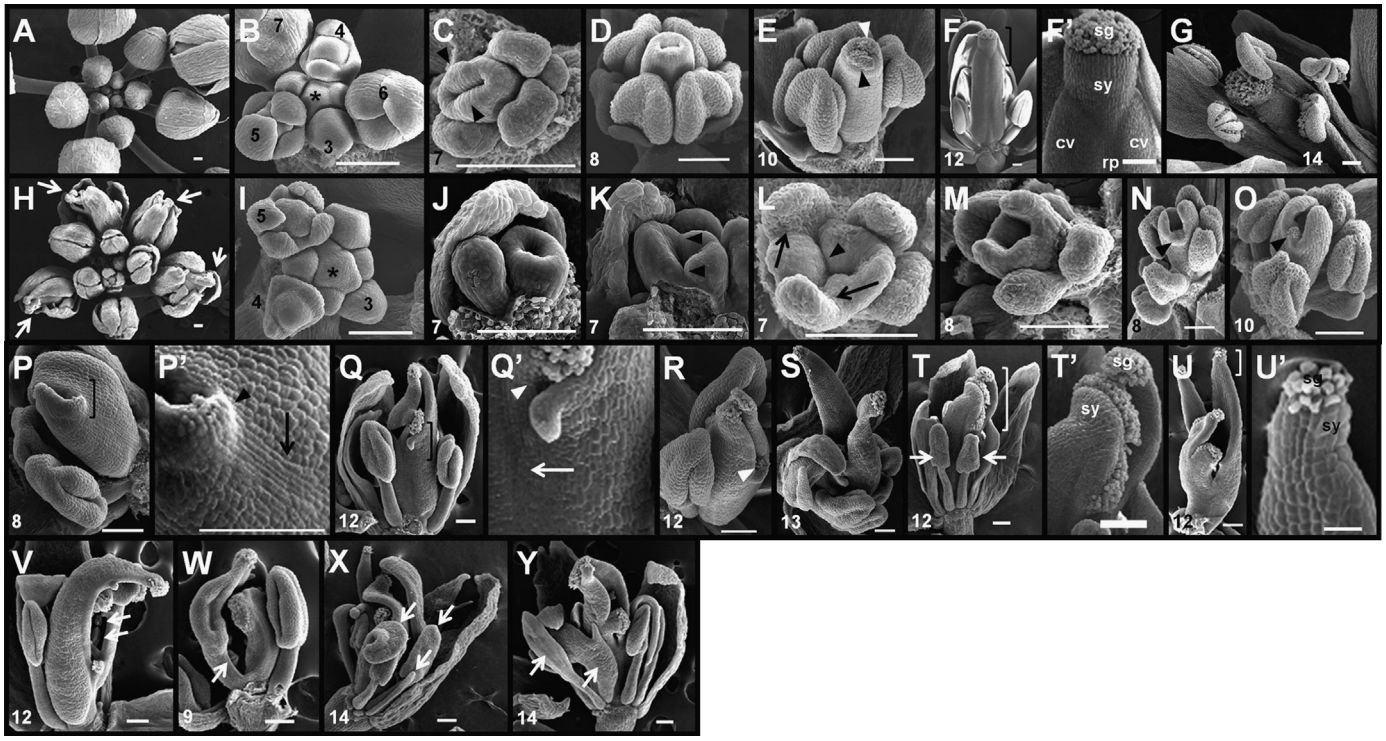

Fig. 1. Analysis of gynoecium and anther development by SEM. (A)–(G) The wild-type phenotypes. The numbers in the images denote the flower stages (Smyth et al., 1990). (A) and (B) Top views of inflorescence. Asterisks indicate the inflorescence meristem. (C) Medial ridges (arrowheads) of the gynoecium with a slot. (D) Elongating gynoecium with anthers. (E) Developing medial papillae on the stigma (arrowheads). (F) and (F′) Mature gynoecium; the prime-labeled picture shows a magnified version of the bracketed portion: stigma (sg), style (sy), carpel valves (cv), and replum (rp). (G) Dehiscent anthers releasing pollen. (H)–(Y) The *gif*1 *gif*2 *gif*3 mutant phenotypes. H and (I) Top views of inflorescence. Arrows indicate split gynoecia. (J) Gynoecial cylinder with no medial ridge. (K) and (L) Medial regions with clefts (arrowheads) and some stamens fused to the gynoecium (arrows). (M)–(O) Elongating carpel valves with precociously developing papillar tissues (arrowheads). (P)–(Q′), Gynoecium with papillae (arrowheads) and the replum (arrows). (R)–(U′) Carpel valves topped with style and stigma; precocious papillae (arrowhead); flat stamens (arrows). (V) and (W) Exposed ovules (arrows). (X) and (Y) Aberrant second- and third-whorl floral organs (arrows). Scale bars = 100 μm.

stages of gynoecium development, two medial ridges are formed on the adaxial (inner) and medial portions of the gynoecial cylinder, giving rise to the CMMs (Fig. 1C).

As for the *gif* triple mutant, its flower primordia were, apparently, indistinguishable from the wild type until stage 5 (Fig. 1I). However, the mutant gynoecial cylinder at stage 7 lacked typical medial ridges (Fig. 1J). Afterwards, the apical rim of the mutant cylinder was jagged, displaying clefts: some gynoecia had clefts at both medial sides, some only at one side (Fig. 1K and L). In addition, developing stamens often fused to the gynoecial cylinder (Fig. 1L and W). The clefts became deeper as the gynoecial cylinder elongated, rendering the gynoecial apex split (Fig. 1M–O). The carpel valves continued to grow and formed one-horn-shaped or two-horn-shaped gynoecia (Fig. 1M–Y). Close examination of the basal adjoining region between the split valves revealed that the region always corresponded to the upper edge of the presumptive replum and that the cells in the region precociously differentiated into papillar cells (Fig. 1N, O, P, P′, Q, Q′ and R). Sometimes the mutant gynoecium formed additional minor valves (Fig. 1U). It should be noted that carpel valves were always topped with the stigmatic papillae and style tissues (Fig. 1Q–Y).

The *gif* triple mutant also displayed severe structural defects in the anther. Whereas the wild-type anther had a four-lobed structure with a bilateral symmetry, releasing pollen grains at dehiscence (Fig. 1D, E and G), most of mutant anthers developed poorly, so that their lobes were obscure or flattened (Fig. 1Q, T and X). The mutant anthers often fused to carpels or petals (Fig. 1W and Y). Some anthers developed a four-lobed structure apparently, but showed no sign of dehiscence and pollen grains (also see below). The *gif* double mutations caused no obvious structural aberrations in the gynoecium and the anther (Table 1; data not shown). These results altogether indicate that the *GIF*1 to *GIF*3 genes are necessary for normal development of the gynoecium and the anther in a functionally redundant manner.

Interior defects in the gynoecium of the gif triple mutant

We performed histological analysis in order to examine internal structures of the gynoecium. The early gynoecial cylinder of the wild-type plant showed typical medial ridges that were strongly stained by toluidine blue, because the CMM cells had dense cytoplasm (Fig. 2A). The medial ridges grew further inwards to meet each other and fused together, establishing the septum (Fig. 2B–D). Concomitantly, the flanking regions of the medial ridges take on the placental activity, from which ovule primordia are formed, develop, and, finally, bear the embryo sac (Fig. 2B–E).

In the *gif* triple mutant, however, we found severe structural and functional defects in the CMM tissues. In more than 70% of the early mutant gynoecia, only a single medial ridge developed normally, whereas the other split in the middle (Fig. 2K). Less frequently, the mutant gynoecium had both medial ridges split (Fig. 2O). The marginal region of the split medial tissue always produced a papillar tissue precociously (Fig. 2P). As such, the mutant gynoecium, beyond the split region, lacked the replum and the septum that were to be derived from the CMM, having only a single replum and the half septum (Fig. 2Q). Sometimes the residual part of split medial ridges produced ovules (Fig. 2R; also see Fig. 1Q′). It is noteworthy that, even in the unsplit region of the gynoecium, medial ridges rarely met together to form a complete septum, indicating that the surviving CMMs retained only a partial functionality (Fig. 2S). Interestingly, serial sections of the medial ridge region showed that the meristematic cells in the split region developed into smaller cells compared with neighboring cells and the cells underneath them (Fig. 2K–N). Taken together, it seems that mutant CMMs failed to maintain their meristematic competence.

Structural defects in the ovule of the gif mutants

Wild-type ovules arise as a finger-like primordium from the placenta, after which inner and outer integuments initiate at the chalaza (Fig. 3A and B). Inner integuments start to form as a ring of cells around the chalazal circumference and exhibit a cylindrical growth pattern until they surround and, eventually, encase the nucellus (Fig. 3B–E). Outer integuments also initiates from the chalazal cells underneath the ring of inner integument cells, gynobasal side first (the side toward the base of the ovary) and gynoapical side next (Fig. 3B). The differential growth pattern is the earliest morphological sign that the gynoapical–gynobasal polarity is established in the chalazal region and thus in the developing ovule (Sieber et al., 2004). Outer integument cells proliferate faster than inner ones do, completely enveloping inner integuments and the nucellus (Fig. 3C–F).

Fig. 3G presents the internal structure of the split gynoecium of the *gif* triple mutant: the transverse, convex medial ridge did not establish the septum, but bore ovule primordia from the placental regions. Mutant ovules appear to be normal at initiation stage, but form integuments in a less organized manner, leaving a gap between inner and outer integuments (Fig. 3H, I and K). Frequently, the ring layer of inner integuments was not completely formed, leaving a gap (Fig. 3J, L and M). Inner integuments continued to grow until their final stage, but failed to wrap the nucellus completely; the outer integument growth was also retarded, exposing inner integuments (Fig. 3K–M).

In the wild-type ovule, the gynobasal portion of both integuments grows faster than the gynoapical portion, positioning the mycropyle adjacent to the funiculus, i.e., forming the anatropous ovule (Fig. 3F; Modrusan et al., 1994). Yet, *gif*1 *gif*2 *gif*3 triple mutant integuments lost the capability to grow asymmetrically, resulting in a linear ovule form that resembles an orthotropous type (Fig. 3L and M). The growth or polarity defect is more evidently illustrated in DIC micrographs (Fig. 4). Wild-type integuments show an asymmetric growth pattern: the leading growth at the gynobasal side and the lagging growth at the gynoapical side (Fig. 4A and WT row). In contrast, the *gif*1 *gif*2 *gif*3 integuments lose the asymmetric growth property from the earliest stages of ovule development and are also remarkably small even at their final stage, failing to fully enclose the nucellus (Fig. 4A and gif1/2/3 row). Moreover, the presence of the embryo sac was not detected in the *gif*1 *gif*2 *gif*3 ovules (also see below). Integuments of the *gif*1 single mutant displayed the asymmetric growth pattern, but to a slightly lesser extent (Fig. 4A and gif1 row). Integuments of the *gif*1 *gif*2 double mutant showed a significantly reduced asymmetric growth, putting the micropyle at the right angle to the funiculus (Fig. 4A and gif1/2 row). It is noteworthy that the *gif*1 *gif*2 embryo sac protruded out from the ovule.

When cells in the outermost layer of integuments were counted, we found that the *gif* mutants had significantly reduced cell numbers that correlated with the mutation dosages (Fig. 4B and C). These results indicate that the retarded growth of mutant integuments is due to a reduction in the cell proliferation. Therefore, we suggest that the *GIF* genes are necessary for the cell proliferation and, perhaps, polarity maintenance of ovules as well as for formation of the embryo sac.

Defective sporogenesis and gametogenesis of the gif triple mutant

The female gametogenesis starts from the archesporial cell, which directly differentiates into the MMC in *Arabidopsis* (Webb and Gunning, 1990). Fig. 2F and G shows the presence of the archesporial cell and MMC in the wild-type ovule. The MMC divides meiotically to produce four haploid megaspores in the nucellus, among which three distal megaspores degenerate and only the chalazal megaspore develops into the functional megaspore (FMS) (Fig. 2H; Webb and

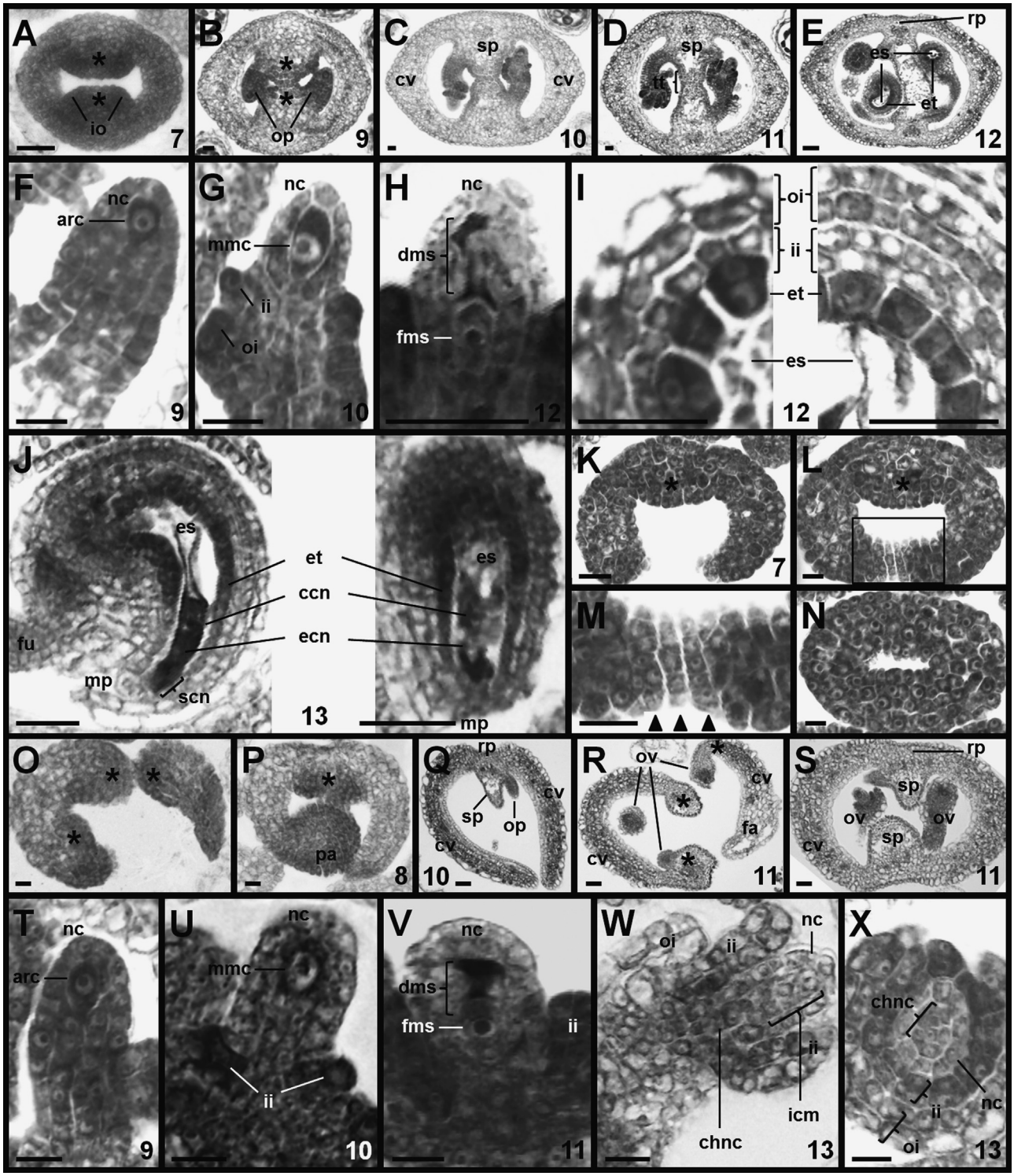

Fig. 2. Histological analysis of gynoecium and ovule development. (A)–(J) Normal development of the wild-type gynoecium and ovule. (K)–(X) Developmental defects of the *gif*1 *gif*2 *gif*3 gynoecium and ovule. The numbers in the images indicate the flower stages. Asterisks indicate the medial ridges. arc, archesporial cell; ccn, central cell nucleus; chnc, chalaza-side nucellus; cv, carpel valve; dms, degenerating megaspore; ecn, egg cell nucleus; es, embryo sac; et, endothelium; fa, fused anther; fms, functional megaspore; fu, funiculus; icm, inner cell mass; ii, inner integument; io, incipient ovule; mmc, megaspore mother cell; mp, micropyle; nc, nucellus; oi, outer integument; op, ovule primordium; ov, developing or mature ovule; pa, papillae; rp, replum; scn, synergid cell nucleus; sp, septum; tt, transmitting tract. Scale bars = 10 μm.

Gunning, 1990; Robinson-Beers et al., 1992; Modrusan et al., 1994). The FMS performs three consecutive mitotic divisions to form the embryo sac/female gametophyte (Fig. 2J; Yadegari and Drews, 2004). During that time, some cells of the nucellus degenerate, and the embryo sac enlarges and fills the nucellar space. Note that wild-type embryo sacs are surrounded by a single layer of densely stained endothelial cells, except around the micropylar region (Fig. 2E and J). The endothelial cells are formed by periclinal division of the innermost cells of integuments around flower stage 12 (Fig. 2I).

The *gif*1 *gif*2 *gif*3 ovule, like the wild type, developed the archesporial cell and the MMC as well as the FMS with concomitant degeneration of the other three distal megaspores (Fig. 2T–V),

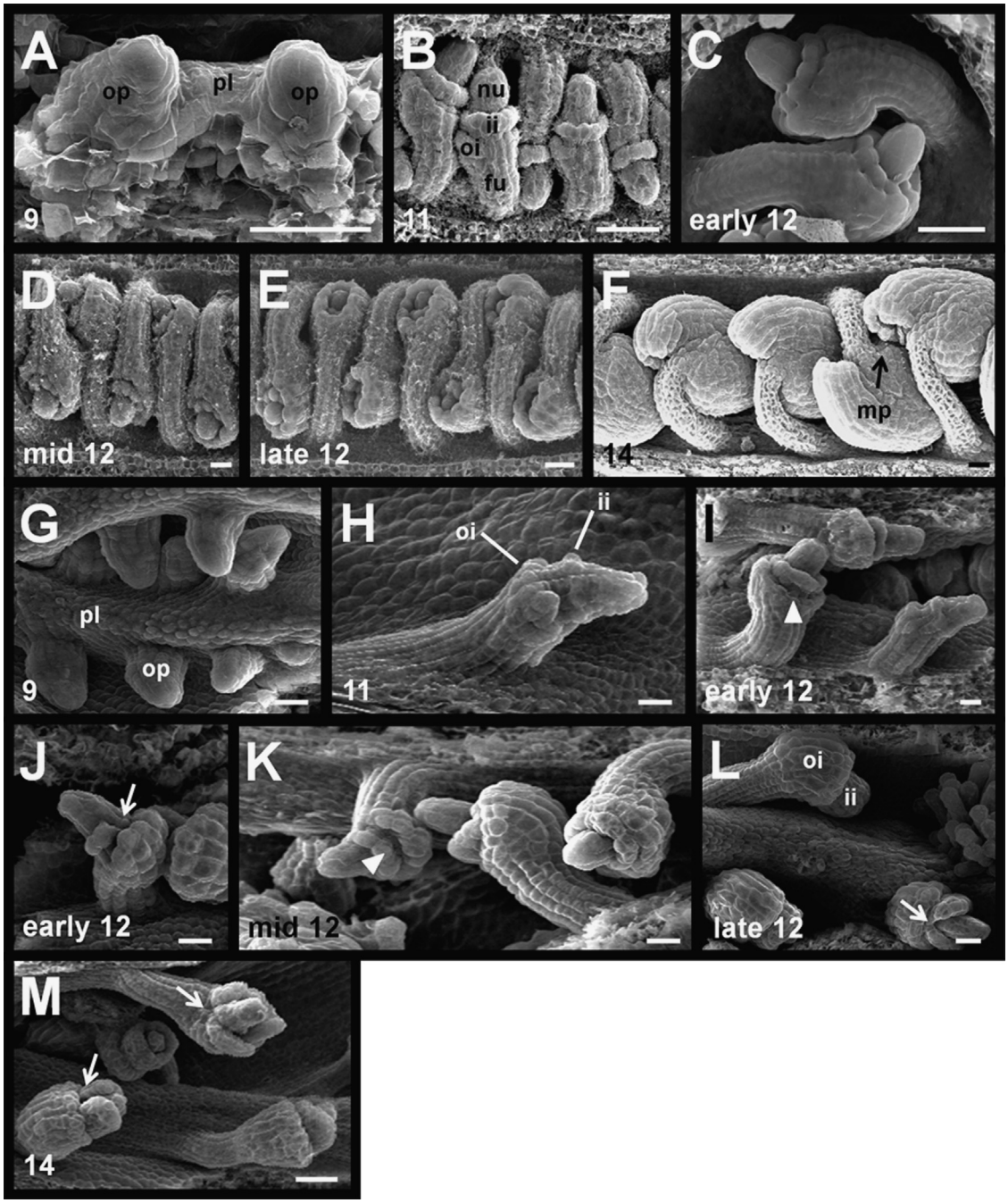

Fig. 3. Analysis of ovule development by SEM. (A)–(F) The wild-type ovules. (G)–(M) The *gif*1 *gif*2 *gif*3 ovules. The numbers in the images indicate the flower stages. Arrowheads indicate a gap between inner and outer integuments; arrows, split inner integument. ii, inner integument; fu, funiculus; mp, mycropyle; nu, nucellus; oi, outer integument; op, ovule primordium; pl, placenta. Scale bars=20 μm.

indicating that the *gif* mutations did not affect the megasporogenesis. However, we failed to find even a single mature embryo sac in more than one hundred ovules examined. Instead, the mutant ovule retained the nucellus with a cellular mass of uncertain identity (Fig. 2W and X). Mutant ovules also lacked the endothelial layer. The results indicate that the *gif* triple mutation caused female gametogenesis to abort after the female sporogenesis and also reduced the periclinal divisional activity of the innermost integument.

The male gametogenesis starts from the archesporial cells that are specified in the L2 layer of the stamen primordium (Sanders et al., 1999). The wild-type anther at the stamen stage 2 establishes the archisporial cells in its four corners (Fig. 5A). The archesporial cells divide to generate the primary parietal and primary sporogenous cells, and, afterwards, the former divides periclinally to produce two layers of the secondary parietal cells, and the latter differentiates into PMCs (Fig. 5B). Following another round of periclinal division of the inner layer of the secondary parietal cells, the anther establishes the microsporangium that consists of three concentric layers: endothecium, middle layer, and tapetum (Fig. 5C). The PMC undergoes meiosis to generate the tetrads, i.e., four haploid cells that differentiate into microspores and, finally, pollen grains (Fig. 5D–G).

In contrast to the wild type developmental progression, most anthers of the *gif* triple mutant were structurally malformed, and contained only connective and vascular tissues without any

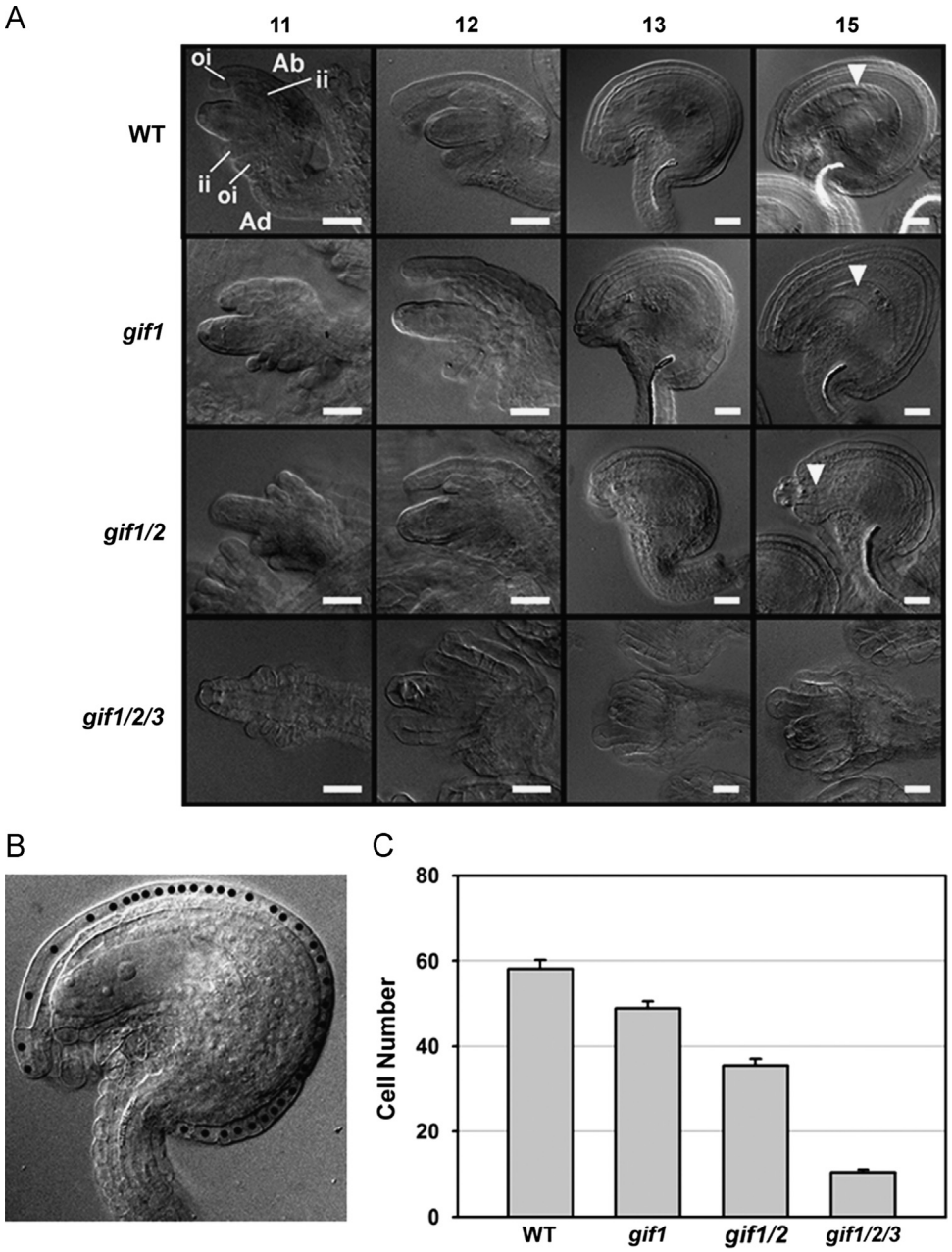

Fig. 4. Analysis of ovule development by DIC microscopy. (A) Images of developing ovules under the DIC. The numbers on top indicate the flower stages; the marks on each row, genetic background. Ab, gynobasal side; Ad, gynoapical side; ii, inner integuments; oi, outer integuments. The arrowheads indicate the embryo sac. Scale bars = 10 μm. (B) Individual cells of the outermost layer of the integuments were dotted for determination of the cell number. (C) Cell numbers of the outermost integuments of the wild-type and mutant plants.

microsporangium or pollen grains (Fig. 5H). Nonetheless, the mutant anther clearly harbored the archesporial cells, which produced progeny cells that were to be the primary parietal and primary sporogenous cells (Fig. 5I and J). Yet, both the primary progeny cells were highly vacuolated and seldom culminated in formation of the microsporangium and pollen, resulting in only connective cells (Fig. 5J–L). The results suggest that the primary progeny of the archesporial cells failed to maintain their specification identity. The archesporial lineage cells, on occasion, managed to form the microsporangium, but the surviving tapetal cells and PMCs became vacuolated (Fig. 5M and N). The results indicate that the *GIF* gene family is absolutely required for maintenance of the archesporial lineages and thus for production of pollen grains. Only rarely are intact microsporangia and functional PMCs that produced viable pollen grains observed in the *gif* 1 *gif2 gif3* mutant (Fig. 5O–Q).

In situ localization of GIF mRNAs

In order to investigate the expression patterns of the *GIF* genes in floral organs, we performed in situ localization of *GIF* mRNAs (Fig. 6). Both *GIF*1 and *GIF*2 transcripts were detected throughout the flower buds at flower stages 1 and 2, but then began to be expressed more strongly in more peripherial portions of the stage 3 flower bud (in the presumptive sepal primordia) (Fig. 6A and I). During stages 6 through 9 the *GIF*1 and *GIF*2 transcripts were detected strongly in the incipient primordia and microsporangial portions of the anthers, where the archesporial cells and PMCs reside (Fig. 6B, F, G, J, K and L). Later on, expression of *GIF*1 and *GIF*2 was detected in the meiotic cells, microspores and tapetal cells (Fig. 6H and N). The *GIF*1 signal also appeared in the gynoecium, especially in its presumptive carpel valves starting at

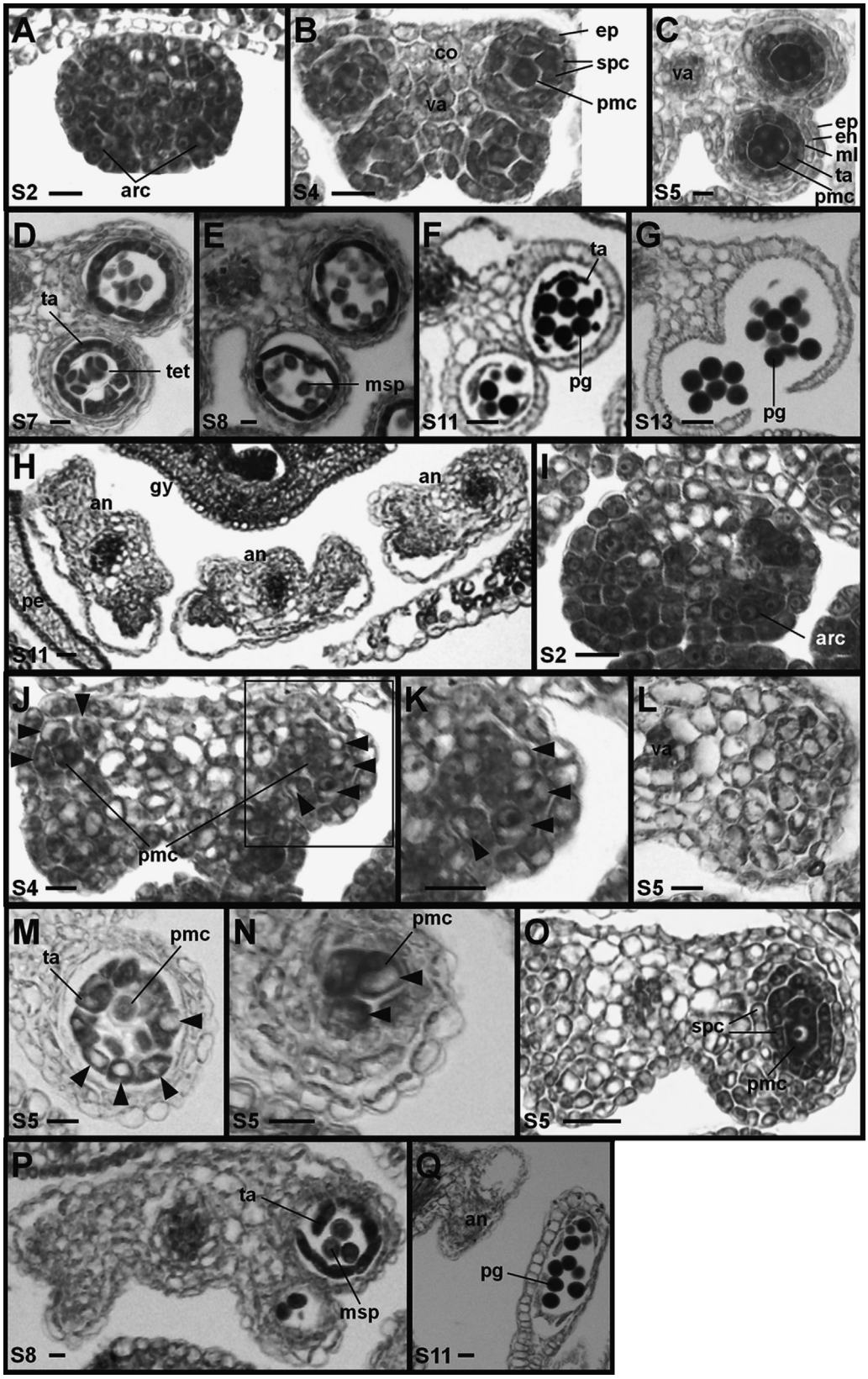

Fig. 5. Histological analysis of anther development. (A)–(G) Normal development of the wild-type anther. (H)–(Q) Developmental defects of the *gif*1 *gif*2 *gif*3 anther. The numbers in the images indicate developmental stages of the stamen (Sanders et al., 1999). The arrowheads mark vacuolated cells. an, anther; arc, archesporial cell; co, connective tissue; en, endothecium; ep, epidermis; gy, gynoecium; ml, middle layer; msp, microspore; pe, petal; pg, pollen grain; pp, primary parietal cell; pmc, pollen mother cell; se, sepal; sp, sporogenous cell; spc, secondary parietal cells; ta, tapetum; tet, tetrads; va, vasculature. Scale bars = 10 μm.

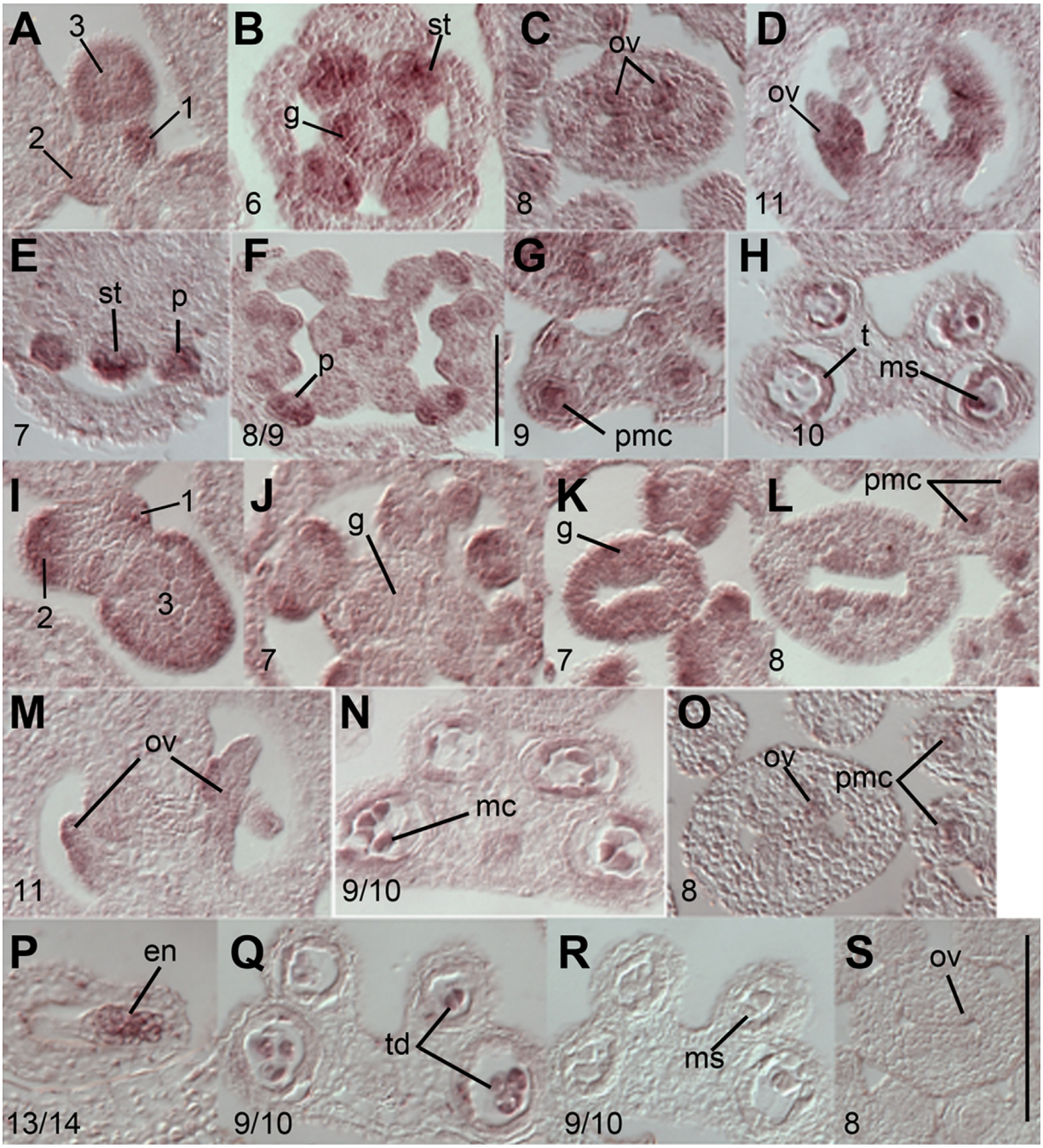

Fig. 6. Expression patterns of *GIF*1, *GIF*2, and *GIF*3 in developing flowers. All panels display in situ hybridization results from wild-type floral cross sections. (A)–(H) *GIF*1 antisense probe. (I)–(N) *GIF*2 antisense probe. (O)–(Q) *GIF*3 antisense probe. (R) and (S) Representative images resulting from *GIF*1 to *GIF*3 sense probes, displaying low background. The numbers indicate the flower stages (Smyth et al., 1990). en, endosperm; g, gynoecium; mc, meiotic cell; mr, microsporangial region; ms, microspores; ov, ovule; p, petal primordium; pmc, pollen mother cell; st, stamen primordium; t, tapetum; td, tetrads. The scale bar drawn in panel (S) represents 100 μm for all panels except for panel (F). The scale bar indicated in panel F represents 100 μm for that panel.

early stage 7 (Fig. 6B). Expression of the *GIF*2 transcript was clearly stronger at more apical portions of the gynoecium relative to more basal portions of the same gynoecium during stage 7 (Compare Fig. 6J with K: these two sections are 40 μm apart in the same flower bud). *GIF*1 and *GIF*2 transcripts were also detected in ovules as they began to arise from the placental tissue during stage 8 (Fig. 6C and L). As the ovules matured, the *GIF*1 and *GIF*2 expression was strongly observed in the chalazal portions of the ovule and in the initiating and developing integuments (Fig. 6D and M). As the growth of the integuments was completed, expression within the ovules declined. Expression was subsequently detected in the developing seed in what is we believe is endosperm nuclei, although it was difficult to ascertain the identity of the tissue due to the poor fixation of the non-cellularized endosperm at this developmental stage (data not shown and Fig. 6P for *GIF*3). In general, the signal from the *GIF*3 probe was significantly weaker than that observed from the *GIF*1 and *GIF*2 probes. Expression of the *GIF*3 probe could not be detected above background in the early flower stages 1–6; data not shown). Starting at stage 8, however, *GIF*3 signal was weakly detected in PMCs of the anthers and in ovule primordia (Fig. 6O). Later on, the *GIF*3 signal was detected in tetrads (Fig. 6Q) and in the embryo sac, probably in endosperm (Fig. 6P). In summary, the expression patterns of the *GIF* genes as determined by in situ

hybridization were highly correlated with the developmental defects in the *gif* triple mutant.

Localization patterns of the GIF::GUS fusion proteins

Using translational *GIF*::*GUS* reporter fusion constructs, we examined the spatio-temporal localization of GIF proteins. For preparation of the reporters, the whole genomic sequence of the *GIF* genes, including their own promoter, introns, and exons, was fused in frame to the *GUS* coding sequence (see Materials and methods section for detail). When incubated in a GUS staining solution for 7 h, the *GIF*1::*GUS* translational reporter line (*GIF*1*pro*::*GIF*1::*GUS*) showed a strong staining signal in the apical portion of the gynoecial primordium, but was not detected at more basal positions (Fig. 7A and B). A cross section image reveals that the signal was localized in inner layers of the presumptive carpel valves (Fig. 7D1). At flower stage 12, the signal was detected again in the stigmatic tissues and inner layers of carpel valves (Fig. 7C). It should be noted that with a prolonged incubation (16 h) the signal was detected in the whole gynoecium, including the ovule primordium (Fig. 7D2). However, at later stages the signal was restricted to the ovule and the embryo sac or perhaps endosperm (Fig. 7D3 and D4). The signal was also detected in the anther, albeit weakly even with the prolonged incubation: first, overall in the anther primordium, then in the archesporial lineage cells, including tapetal cells and PMCs, and, finally, in pollen grains (Fig. 7E1–F).

As for the *GIF2pro*::*GIF2*::*GUS* line, the staining signal was detected in the ovule and papillae, but not in the gynoecium at early stages (Fig. 7G–J1). Yet again, a prolonged incubation rendered the whole gynoecium stained, including the ovule and embryo sac (Fig. 7J2–J4). The staining pattern of the anther was similar to that of the *GIF*1*pro*::*GIF*1::*GUS*, with exceptions that the signal was distinctive in the tapetum and filament but very weak in pollen grains (Fig. 7K1–L).

The *GIF3pro*::*GIF3*::*GUS* line displayed a strong signal in the whole gynoecial primordium, subsequently being constrained to the uppermost tissue and, later on, expanding to the style and the upper region of the ovary, but not in the stigmatic papillae (Fig. 7M–O). Interestingly, a cross section revealed that the medial ridges of the gynoecial primordium were more strongly stained than the rest parts of the gynoecium (Fig. 7P1). With a prolonged incubation, the whole gynoecium was stained (Fig. 7P2). Eventually, however, the signal became very weak in mature gynoecium that it was difficult to detect (Fig. 7P3 and P4). The staining patterns in the *GIF3pro*::*GIF3*::*GUS* anther were also similar to those of other *GIF*::*GUS* reporter lines (Fig. 7Q1–R).

In summary, the spatial and temporal localization patterns of GIF::GUS proteins virtually overlap with each other and largely match those of their transcripts as detected by in situ hybridization. It should be noticed, however, that the GIF2::GUS proteins accumulated in a more localized fashion compared with that of *GIF2* mRNA, and that the localization patterns of *GIF3* mRNAs only minimally overlapped those of GIF3::GUS fusion proteins. The discrepancies may be the result of the differential sensitivity of the two methods, a lack of some promoter/enhancer elements in the reporter constructs (See Supplementary Fig. 1) or real differences between the accumulation of the transcript and the fusion protein.

Discussion

The GIF family is required to maintain the meristematic specification state of the CMM and its derivative cells

Carpel margins of the *gif*1 *gif*2 *gif*3 loss-of-function mutant failed to fuse along the medial domain, resulting in split gynoecium. The defect appeared shortly after the gynoecial primordium initiated, because its medial ridges lost their capacity to grow (Fig. 1). In detail, the presumptive replum tissue ceased to grow, and its distal region precociously formed the stigmatic papillae. In addition, no additional CMM-derived structures (the septum,

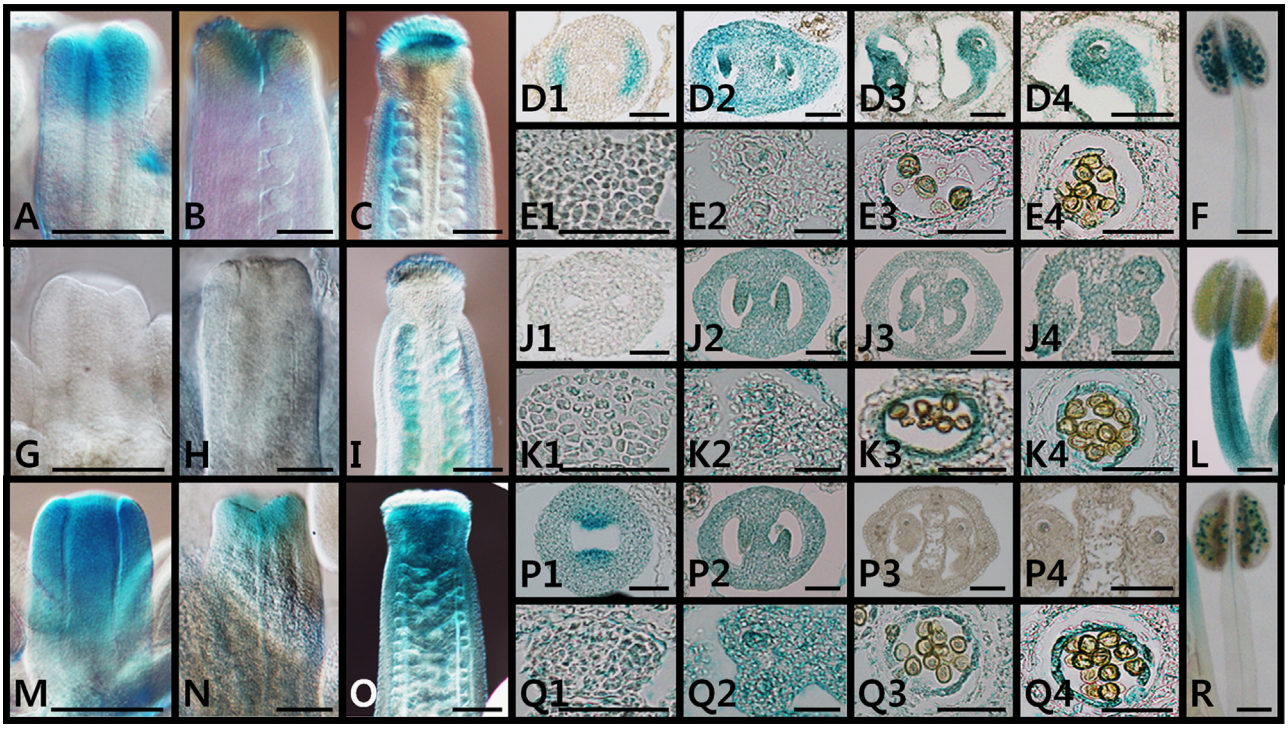

Fig. 7. Localization of GIF::GUS fusion proteins. (A)–(F) The GUS staining patterns of *GIF*1*pro*::*GIF*1::*GUS* reporter line; (G)–(L) *GIF2pro*::*GIF2*::*GUS*; (M)–(R) *GIF3pro*::*GIF3*::*GUS*. Flower clusters were incubated with a GUS staining solution for the indicated time: 7 h for (A)–(D1) and (G)–(J1); 2 h, (M)–(P1); 16–24 h for the rests. The whole mount of the gynoecium was examined under the DIC; tissue sections were imaged under a light microscope. Scale bar=50 μm.

the placenta, and the ovule) initiated beyond the split point (Figs. 1 and 2; Table 1). These results clearly indicate that the *GIF* family is essential for development of the CMM and its derivatives.

What is the biological function of the *GIF* family in this process? Histological analysis revealed that a portion of the mutant CMM cells became smaller and precociously differentiated into the medial stigmatic papillae, which is an ultimate fate of the CMM cells (Figs. 1 and 2). Therefore, the *GIF* genes may function to maintain meristematic competence of the CMM cells, thereby preventing them from precocious differentiation. This would thus support active cell proliferation and the coordinated growth between the medial and lateral domains of the gynoecium. The interpretation can be extended to other developmental aberrations of the triple mutant. Inner and outer integuments of the *gif*1 *gif*2 *gif*3 ovule prematurely lose their mitotic competence, thus fail to achieve their full size, and fail to contain the full complement of integument cells (Figs. 3 and 4). Similarly, the innermost layer of the mutant integuments lacked the periclinal divisional activity that leads to formation of the endothelium (Fig. 2). Even the FMS in the ovule lost its due fate as a progenitor cell of gametophytic cells and thus failed to perform the megagametogenesis, whereas the archesporial cell underwent normal megasporogenesis, producing the FMS (Fig. 2T–X). It should be, however, noted that it is not clear at present whether the FMS lost its mitotic potency (leading to no progeny) or its identity (producing non-gametophytic cells), since the mutant nucellus contained an inner mass of cells whose origin and identity was intractable in our analysis. Taken together, our interpretation is well supported by the results that the *GIF* genes are expressed, actively and dynamically, in those meristematic tissues of the gynoecium (Figs. 6 and 7). Alternatively, however, we cannot rule out the possibility that the failure to properly develop the female gametophyte may be due to an indirect effect on integument growth rather than a direct result of the loss of *GIF* activity within the developing female gametophyte.

It is an interesting syndrome that the mutant integuments experience a loss of the gynobasal/gynoapical growth polarity and a reduction in the cell proliferation (Figs. 3 and 4). The *gif* triple mutation seems to bring in the polarity loss by reducing the cell proliferation activity of integuments, rather than be directly involved in the polarity establishment. The interpretation is compatible with the result that the *an*3-4 mutation, a loss-of-function allele of *GIF*1/*AN*3, did not affect the expression patterns of various adaxial/abaxial identity genes in the leaf primordium, although the *an*3-4 mutation enhanced adaxial defects in the *asymmetric leaves*1 (*as*1) and *as*2 mutants (Horiguchi et al., 2011). In a conservative explanation, it is obvious that the integumental growth is dependent on the cell proliferation activity promoted by the *GIF* genes.

A number of genetic factors are required for formation and activities of the CMM tissues in *Arabidopsis* (Ferrándiz et al., 1999, 2010). Among those, *LEUNIG, SEUSS* (*SEU*), *AINTEGUMENTA* (*ANT*), and *FILAMENTOUS FLOWER* play pivotal roles in the developmental process. All the single mutants corresponding to these genes share a common structural defect, weak or strong, in the CMM tissues, and their double combinations brought about split gynoecia and, internally, produced almost no septum, placenta, and ovule (Liu and Meyerowitz, 1995; Chen et al., 2000; Krizek et al., 2000; Franks et al., 2002; Azhakanandam et al., 2008). The results indicate that these gene products exert an overlapping function in the CMM tissues, perhaps forming a multimeric complex together (Nole-Wilson and Krizek, 2006; Azhakanandam et al., 2008). Our present study clearly showed that the CMM phenotype of the *gif* triple mutant was similar, albeit less severe, to that of these double mutants. It is, therefore, conceivable that the *GIF* family may exert a redundant function in the context of the known genetic network. However, we have found no significant evidence for a genetic interaction in regard to the carpel and ovule development when the *gif*1 single mutant was crossed to other mutants, such as the *ant*-1 and *seu*-3 (Supplementary Fig. 2A and B). Nonetheless, we found a synergistic reduction in leaf growth of the *gif*1 *ant*-1 double mutant, compared with its parental single mutants. The results indicate that the GIF1 and ANT signaling pathways may be somehow associated in regard to leaf growth, and also raise the possibility that a higher order of mutational combinations, including *gif*2 and *gif*3, may disclose a clue for a genetic interaction with respect to reproductive organ development.

The GIF family is required to maintain the specification state of archesporial lineage cells in the anther

Although the *gif*1 *gif*2 *gif*3 anther formed normal archesporial cells, their immediate progeny became highly vacuolated and differentiated into the connective cells, establishing no microsporangium and pollen grains (Fig. 5). Sometimes the tapetum cells and PMCs survived, but they were also subjected to the same degenerative fate as the immediate progeny. Eventually, the whole anther consisted of only the connective cells. Therefore, the notion that the *GIF* function is critical for maintenance of the cell fate specification fits in best with development of the archesporial lineages, i.e., the parietal and sporgenous cells. This is well in line with the expression patterns of the *GIF* genes: they are expressed not only in the incipient anther but also in the archesporial cells and their progeny, including the tapetum, PMCs, and pollen (Figs. 6 and 7).

To date, a host of protein factors have been known to be involved in the anther development: SPOROCYTELESS/NOZZLE (SPL/NZZ), EXCESS MICROSPOROCYTES1/EXTRA SPOROGENOUS CELLS (EMS1/EXS), SOMATIC EMBRYOGENESIS1 (SERK1), SERK2, TAPETUM DETERMINANT1 (TPD1) RECEPTOR-LIKE PROTEIN KINASE2 (RPK2), DYSFUNCTIONAL TAPETUM1 (DYT1), BARELY ANY MERISTEM1(BAM1), and BAM2 ((Schiefthaler et al., 1999; Yang et al., 1999, 2003, 2005; Canales et al., 2002; Zhao et al., 2002; Ito et al., 2004; Albrecht et al., 2005; Colcombet et al.,2005; Hord et al., 2006; Zhang et al., 2006; Mizuno et al., 2007; Zhu et al., 2008). Among them, the *SPL* gene has a pivotal importance. The *spl* mutant anther comprises only connective cells, because both the parietal and sporogenous cells become vacuolated and differentiated (Yang et al., 1999), suggesting that the SPL MADS box transcription factor specifies and maintains the sporogenous cell fate. Other mutations, such as *ems*1/*exa*, *serk*1 *serk*2, and *tpd*1, caused similar specification defects, but in a specific layer, i.e., the tapetum, indicating that the EMS1 signaling is necessary for the tapetal cell fate (Canales et al., 2002; Zhao et al., 2002; Yang et al., 2003, 2005; Albrecht et al., 2005; Colcombet et al.,2005; Feng and Dickinson, 2010). The *dyt*1and *rpk*2 mutants also develop highly vacuolated tapetal cells (Zhang et al., 2006; Mizuno et al., 2007). Although the *DYT* gene was suggested to act downstream of *SPL*/*NZZ* and *EMS*1/*EXA*, it was not sufficient for the tapetum development, suggesting that additional genes are necessary at the downstream signaling pathway of *SPL*/*NZZ* and *EMS*1/*EXA*.

It is interesting that a common phenotype of all of the mutants corresponding to those genes is a failure in the specification and maintenance of the parietal and/or sporogenous cell fate. In this study, we discovered that the *GIF* family also played an essential role in the fate maintenance of the archesporial lineage cells. It seems that the whole differentiation event from the archesporial cells to the parietal and sporogenous lineage cells requires the presence of active GIF proteins. Therefore, it is a tempting speculation that GIF proteins may be associated with those existing regulatory networks.

Molecular mechanism of the GIF function

How do the GIF proteins maintain the cell specification? To date, no experimental evidence has been given to understand the molecular mechanisms by which the GIF transcriptional co-activators exert their effect. Horiguchi et al. (2011) provided a list of genes whose expression was down- or up-regulated in the leaf primordium of the *an*3-4 allele, which may provide an important experimental platform for elucidation of the action mechanism of the *GIF* genes. Recently, the GIF1/AN3 protein was demonstrated to have a capacity to move across cells via plasmodesmata, thus balancing the cell proliferation activities of leaf epidermal and subepidermal tissues (Kawade et al., 2010, 2013), and the result gives an important clue about the molecular mechanism of the GIF action.

The GIF transcriptional co-activators form a functional complex with the GRF transcriptional factors to regulate leaf growth (Kim and Kende, 2004; Horiguchi et al., 2005). Therefore, it is highly conceivable that the GRF-GIF duo, not GIF alone, may be involved in development of the reproductive organs. Wynn et al. (2011) listed many genes that might play a role in the CMM development in *Arabidopsis*, and showed that one of nine members of the *GRF* family, *GRF*5, was expressed in the medial portion of the early gynoecium and in the ovule primordium as well as in the early anther primordium. The expression patterns of the *GIF* genes in this study are highly reminiscent of that of *GRF*5 (Fig. 6), supporting this possibility.

Conclusions

Plants continue to produce new cells from meristematic cells during post-embryonic life, thereby forming a variety of new organs, including leaves and flowers, and finally producing the egg and sperm cells. In order to fulfill the tasks, therefore, plants not only have to specify a variety of meristematic cells but also have to maintain their meristematic state. We propose that the GIF protein family is an essential component that enables plants to maintain the competence of meristematic cells to proliferate as seen in the cases of the CMM development. At the same time, the GIF family also plays an essential role in the specification maintenance of the archesprorial lineage cells of the anther. Therefore, the GIF function is of fundamental importance for the reproductive competence and the generation-to-generation continuity of *Arabidopsis* plants.

Acknowledgments

This work was supported by the National Research Foundation of Korea (NRF-2009-0076517 and NRF-2012R1A1A2005100) and by Kyungpook National University Research Fund, 2012.

Appendix A. Supporting information

Supplementary data associated with this article can be found in the online version at http://dx.doi.org/10.1016/j.ydbio.2013.12.009.

References

Albrecht, C., Russinova, E., Hecht, V., Baaijens, E., de Vries, S, 2005. The *Arabidopsis thaliana* SOMATIC EMBRYOGENESIS RECEPTOR-LIKE KINASES1 and 2 control male sporogenesis. Plant Cell 17, 3337–3349.

Azhakanandam, S., Nole-Wilson, S., Bao, F., Franks, R.G., 2008. SEUSS and AINTEGUMENTA mediate patterning and ovule initiation during gynoecium medial domain development. Plant Physiol. 146, 1165–1181.

Bouman, F., 1984. The ovule. In: Johri, BM (Ed.), Embryology of Angiosperms. Springer-Verlag, New York, pp. 123–157.

Bowman, J.L., Baum, S.F., Eshed, Y., Putterill, J., Alvarez, J., 1999. Molecular genetics of gynoecium development in *Arabidopsis*. Curr. Top. Dev. Biol. 45, 155–205.

Canales, C., Bhatt, A.M., Scott, R., Dickinson, H., 2002. EXS, a putative LRR receptor kinase, regulates male germline cell number and tapetal identity and promotes seed development in *Arabidopsis*. Curr. Biol. 12, 1718–1727.

Chen, C.B., Wang, S.P., Huang, H., 2000. LEUNIG has multiple functions in gynoecium development in *Arabidopsis*. Genesis 26, 42–54.

Clough, S.J., Bent, A.F., 1998. Floral dip: a simplified method for Agrobacterium-mediated transformation of *Arabidopsis thaliana*. Plant J. 16, 735–743.

Colcombet, J., Boisson-Dernier, A., Ros-Palau, R., Vera, C.E., Schroeder, J.I., 2005. *Arabidopsis* SOMATIC EMBRYOGENESIS RECEPTOR KINASES1 and 2 are essential for tapetum development and microspore maturation. Plant Cell 17, 3350–3361.

Feng, X., Dickinson, H.G., 2010. Tapetal cell fate, lineage and proliferation in the *Arabidopsis* anther. Development 137, 2409–2416.

Ferrándiz, C., Fourquin, C., Prunet, N., Scutt, C.P., Sundberg, E., Trehin, C., Vialette-Guiraud, A.C.M., 2010. Carpel development. Adv. Bot. Res 55, 1–74.

Ferrándiz, C., Pelaz, S., Yanofsky, M.F., 1999. Control of carpel and fruit development in *Arabidopsis*. Annu. Rev. Biochem. 68, 321–354.

Franks, R.G., Wang, C., Levin, J.Z., Liu, Z., 2002. SEUSS, a member of a novel family of plant regulatory proteins, represses floral homeotic gene expression with LEUNIG. Development 129, 253–263.

Hord, C.L., Chen, C., Deyoung, B.J., Clark, S.E., Ma, H., 2006. The BAM1/BAM2 receptor-like kinases are important regulators of *Arabidopsis* early anther development. Plant Cell 18, 1667–1680.

Horiguchi, G., Kim, G.T., Tsukaya, H., 2005. The transcription factor AtGRF5 and the transcription coactivator AN3 regulate cell proliferation in leaf primordia of *Arabidopsis thaliana*. Plant J. 43, 68–78.

Horiguchi, G., Nakayama, H., Ishikawa, N., Kubo, M., Demura, T., Fukuda, H., Tsukaya, H., 2011. ANGUSTIFOLIA3 plays roles in adaxial/abaxial patterning and growth in leaf morphogenesis. Plant Cell Physiol. 52, 112–124.

Ito, T., Wellmer, F., Yu, H., Das, P., Ito, N., Alves-Ferreira, M., Riechmann, J.L., Meyerowitz, E.M., 2004. The homeotic protein AGAMOUS controls microsporogenesis by regulation of SPOROCYTELESS. Nature 430, 356–360.

Kawade, K., Horiguchi, G., Tsukaya, H., 2010. Non-cell-autonomously coordinated organ size regulation in leaf development. Development 137, 4221–4227.

Kawade, K., Horiguch, G., Usamin, T., Hirai, M.Y., Tsukaya, H., 2013. ANGUSTIFOLIA3 signaling coordinates proliferation between clonally distinct cells in leaves. Curr. Biol. 23, 1–5.

Kim, J.H., Choi, D., Kende, H., 2003. The AtGRF family of putative transcription factors is involved in leaf and cotyledon growth in *Arabidopsis*. Plant J. 36, 94–104.

Kim, J.H., Kende, H., 2004. A transcriptional coactivator, AtGIF1, is involved in regulating leaf growth and morphology in *Arabidopsis*. Proc. Nat. Acad. Sci. U.S. A. 101, 13374–13379.

Krizek, B.A., Prost, V., Macias, A., 2000. AINTEGUMENTA promotes petal identity and acts as a negative regulator of AGAMOUS. Plant Cell 12, 1357–1366.

Lee, B.H., Ko, J-H., Lee, S., Lee, Y., Pak, J-H., Kim, J.H., 2009. The *Arabidopsis* GRF-INTERACTING FACTOR gene family performs an overlapping function in determining organ size as well as multiple developmental properties. Plant Physiol. 151, 655–668.

Liu, Z.C., Meyerowitz, E.M., 1995. LEUNIG regulates AGAMOUS expression in *Arabidopsis* flowers. Development 121, 975–991.

Mizuno, S., Osakabe, Y., Maruyama, K., Ito, T., Osakabe, K., Sato, T., Shinozaki, K., Yamaguchi-Shinozaki, K., 2007. Receptor-like protein kinase 2 (RPK 2) is a novel factor controlling anther development in *Arabidopsis thaliana*. Plant J. 50, 751–766.

Modrusan, Z., Reiser, L., Feldmann, K.A., Fischer, R.L., Haughn, G.W., 1994. Homeotic transformation of ovules into carpel-like structures in *Arabidopsis*. Plant Cell 6, 333–349.

Nole-Wilson, S., Krizek, B.A., 2006. AINTEGUMENTA contributes to organ polarity and regulates growth of lateral organs in combination with YABBY genes. Plant Physiol. 141, 977–987.

Rodrigues-Pousada, R.A., De Rycke, R., Dedonder, A., Van Caeneghem, W., Engler, G., Van Montagu, M., Van Der Straeten, D., 1993. The Arabidopsis 1-aminocyclopropane-1-carboxylate synthase gene 1 is expressed during early development. Plant Cell 5, 897–911.

Reiser, L., Fischer, R.L., 1993. The ovule and the embryo sac. Plant Cell 5, 1291–1301.

Robinson-Beers, K., Pruitt, R.E., Gasser, C.S., 1992. Ovule development in wild-type *Arabidopsis* and two female-sterile mutants. Plant Cell 4, 1237–1249.

Sanders, P.M., Bui, A.Q., Weterings, K., McIntire, K.N., Hsu, Y.C., Lee, P.Y., Truong, M. T., Beals, T.P., Goldberg, R.B., 1999. Anther developmental defects in *Arabidopsis thaliana* male-sterile mutants. Sex. Plant Reprod. 11, 297–322.

Schiefthaler, U., Balasubramanian, S., Sieber, P., Chevalier, D., Wisman, E., Schneitz, K., 1999. Molecular analysis of NOZZLE, a gene involved in pattern formation and early sporogenesis during sex organ development in *Arabidopsis thaliana*. Proc. Nat. Acad. Sci. U.S.A. 96, 11664–11669.

Sieber, P., Gheyselinck, J., Gross-Hardt, R., Laux, T., Grossniklaus, U., Schneitz, K., 2004. Pattern formation during early ovule development in *Arabidopsis thaliana*. Dev. Biol. 15, 321–334.

Smyth, D.R., Bowman, J.L., Meyerowitz, E.M., 1990. Early flower development in *Arabidopsis*. Plant Cell 2, 755–767.

Webb, M.C., Gunning, B.E.S., 1990. Embryo sac development in *Arabidopsis thaliana*. I. Megasporogenesis, including the microtubule cytoskeleton. Sex. Plant Reprod. 3, 244–256.

Wynn, A.N., Rueschhoff, E.E., Franks, R.G., 2011. Transcriptomic characterization of a synergistic genetic interaction during carpel margin meristem development in *Arabidopsis thaliana*. PLoS One 6, e26231.

Yadegari, R., Drews, G.N., 2004. Female gametophyte development. Plant Cell 16, S133–141.

Yang, S.L., Jiang, L., Puah, C.S., Xie, L.F., Zhang, X.Q., Chen, L.Q., Yang, W.C., Ye, D., 2005. Overexpression of TAPETUM DETERMINANT1 alters the cell fates in the *Arabidopsis* carpel and tapetum via genetic interaction with excess microsporocytes1/extra sporogenous cells. Plant Physiol. 139, 186–191.

Yang, S.L., Xie, L.F., Mao, H.Z., Puah, C.S., Yang, W.C., Jiang, L., Sundaresan, V., Ye, D., 2003. TAPETUM DETERMINANT1 is required for cell specialization in the *Arabidopsis* anther. Plant Cell 15, 2792–2804.

Yang, W.C., Ye, D., Xu, J., Sundaresan, V., 1999. The SPOROCYTELESS gene of *Arabidopsis* is required for initiation of sporogenesis and encodes a novel nuclear protein. Genes Dev. 13, 2108–2117.

Zhang, W., Sun, Y., Timofejeva, L., Chen, C., Grossniklaus, U., Ma, H., 2006. Regulation of *Arabidopsis* tapetum development and function by DYSFUNCTIONAL TAPETUM1 (DYT1) encoding a putative bHLH transcription factor. Development 133, 3085–3095.

Zhao, D.Z., Wang, G.F., Speal, B., Ma, H., 2002. The excess microsporocytes1 gene encodes a putative leucine-rich repeat receptor protein kinase that controls somatic and reproductive cell fates in the *Arabidopsis* anther. Genes Dev. 16, 2021–2031.

Zhu, J., Chen, H., Li, H., Gao, J.F., Jiang, H., Wang, C., Guan, Y.F., Yang, Z.N., 2008. Defective in Tapetal development and function 1 is essential for anther development and tapetal function for microspore maturation in *Arabidopsis*. Plant J. 55, 266–277.